Dynamic Stressing of Naturally Fractured Rocks: On the Relation Between Transient Changes in Permeability and Elastic Wave Velocity

Parisa Shokouhi[1], Jiang Jin[1], Clay Wood[2], Jacques Rivière[1], Benjamin Madara[2], Derek Elsworth[2], and Chris Marone[2]

[1]Department of Engineering Science and Mechanics, Pennsylvania State University, University Park, PA, USA, [2]Department of Geosciences, Pennsylvania State University, University Park, PA, USA

Abstract We report on laboratory experiments designed to explore the fundamental processes that impact fluid permeability during drilling and fluid injection. Coupled ultrasonic and permeability measurements are presented for Westerly granite samples fractured in situ and used to illuminate the relationship between nonlinear dynamic stiffness and fracture permeability indexed via fracture aperture. We perturb the effective stress field using normal stress and pore pressure oscillations. The velocity of ultrasonic waves transmitted across the fracture is used to infer the evolution of elastic properties and the fracture nonlinearity. Changes in permeability are measured concurrently. We observe that relative changes in wave velocity and permeability, due to both normal stress and pore pressure oscillations, are correlated, such that larger drops in wave velocity (higher nonlinearity) correspond to larger increases in permeability. Our observations suggest that dynamic stressing is more likely to enhance the permeability of fractures that exhibit greater nonlinearity.

1. Introduction

The injection and recovery of fluids in the subsurface involve significant changes in the local stress field and may cause major changes in the hydromechanical properties of the target reservoir rocks. Of particular concern are dynamic stresses associated with injection, pumping, and transport of fluids. These stresses may pose significant risk associated with accelerated deformation, fault reactivation, and possible damage to reservoir seals. Regional increases in seismic activity induced by such dynamic stresses have been reported in numerous studies (e.g., Brodsky & Lajoie, 2013; Davis & Pennington, 1989; Deichmann & Giardini, 2009; Ellsworth, 2013; Frohlich, 2012; Healy et al., 1968; Holland, 2013; Horton, 2012; McGarr et al., 2015; McNamara et al., 2015; Raleigh et al., 1976; Simpson et al., 1988; Sminchak & Gupta, 2003; van der Elst et al., 2013; Walsh & Zoback, 2015; Weingarten et al., 2015; Zoback, 2012; Zoback & Gorelick, 2012). However, in the context of energy recovery, these dynamic stresses may be beneficial in enhancing permeability and have received relatively little attention.

Transient permeability enhancement caused by dynamic stresses associated with passing seismic waves has been reported at the field scale and also demonstrated in laboratory experiments. These works demonstrate that fluid injection and dynamic stresses combine to produce significant changes in permeability and poromechanical properties of rock (e.g., Elkhoury et al., 2006; Faoro et al., 2009; Elkhoury et al., 2011; Faoro et al., 2012; Candela et al., 2014, 2015; Carey et al., 2015; Frash et al., 2016; Im et al., 2018; Ishibashi et al., 2018; Ye & Ghassemi, 2018; Zhang et al., 2018; Shi et al., 2018; Shi et al., 2019). In addition, other studies have shown that earthquakes and the ensuing seismic waves cause transient changes in rock stiffness in the vicinity of faults (Brenguier et al., 2008; Brenguier et al., 2014; Li et al., 1998, 2006; Niu et al., 2008; Wu et al., 2009). Such observations include coseismic softening of rock as measured by a sudden decrease in seismic wave velocity, followed by a postseismic relaxation in the form of (full or partial) logarithmic recovery with time. Similar behavior has been recorded at laboratory scale, for example, using dynamic acousto-elastic testing (Shokouhi et al., 2017), where wave velocity is measured during dynamic stressing. It is well-established that dynamic perturbations (strain ~10^{-6}) result in a temporary loss of stiffness in so-called nonlinear mesoscopic elastic materials such as rocks (Guyer & Johnson, 2009).
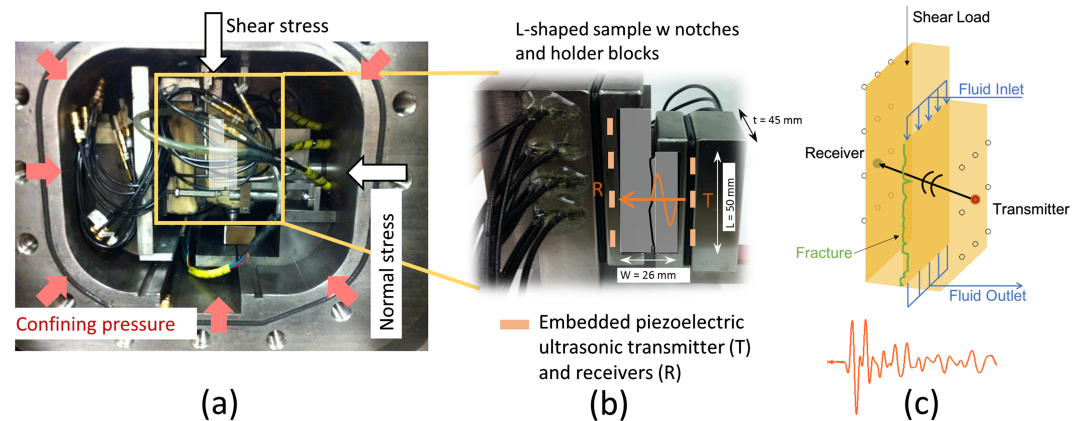
Figure 1. Experimental setup: (a) True triaxial stresses applied to the sample within the pressure vessel; (b) L-shaped sample sandwiched between steel loading blocks with embedded ultrasonic transducers; and (c) schematic representation of the fracture aperture, flow path, and the ultrasonic wave path for a single transmitter-receiver pair together with an example of raw waveform.

The parallels between the observed transient changes in permeability and stiffness due to dynamic stress perturbations suggest a physical link between the nonlinear stiffness and hydraulic characteristics of fractures (e.g., Batzle et al., 2006; Berkowitz, 2002; Berryman et al., 2002; Brown, 1987; Durham & Bonner, 1995; Gale, 1982; Guéguen & Schubnel, 2003; Hofmann et al., 2005; Pyrak-Nolte et al., 1987; Witherspoon et al., 1980; Xu et al., 2006; Zimmerman & Bodvarsson, 1996). In other words, the nonlinear seismic response of fractured rocks is expected to exhibit great sensitivity to features such as fracture roughness and aperture, flow pathways, asperity compliance, and frictional rheology. However, our ability to exploit the nonlinearity in the elastodynamic properties of rock to predict fracture flow and its evolution with time and deformation is limited. Existing studies on coupling between stiffness and poromechanical behavior of fractured samples used quasi-static stress protocols (e.g., Mavko, 2013; Nara et al., 2011; Petrovitch et al., 2013; Pyrak-Nolte & Nolte, 2016). In this paper, we present the results of well-controlled laboratory experiments combining the analysis of nonlinear elastodynamic and hydraulic data.

2. Experimental Setup and Procedure

We conducted experiments with simultaneous measurement of permeability and elastic properties on samples that were fractured in situ under a true triaxial stress state. Samples of Westerly granite were first cut into L-shaped blocks ($68 \times 45 \times 50 \times 26$ mm, Figure 1) and then presaturated with deionized, de-aired water and loaded using steel platens with embedded ultrasonic piezoelectric transducers. The assembly was jacketed in a thin, flexible latex membrane to separate the confining and pore fluids. We independently controlled the confining pressure and the horizontal and vertical applied loads (for details of the sample geometry and apparatus, see Elkhoury et al., 2011; Candela et al., 2014, 2015). The samples were initially intact and were fractured by applying a shear load in servo displacement control (Figure 1). The fracture plane was guided by starter notches at the top and bottom of the sample, which helped in making reproducible, quasi-planar fractures. Shear and normal stresses were applied to the (eventual) fracture plane (Figure 1). Vertical and horizontal displacements of the loading pistons were measured continuously to derive shear and normal components of strain using direct current displacement transducers. An additional linear variable differential transformer (LVDT) was placed inside the pressure vessel to provide precise measurement of displacement normal to the fracture plane. The displacement sensors have an accuracy of ± 0.1 μm.

Two pore pressure intensifiers equipped with LVDTs were used to control fluid pressure (or flow rate) at the top and bottom of the fracture plane (Figure 1). Fluid was introduced along a line source consisting of a narrow channel (45×1 mm) covered by a sintered metal frit and fed by five 1.6-mm diameter holes in order to uniformly distribute the flow along the width of the sample (see Candela et al., 2015).

Each experiment commenced with the application of a small horizontal force followed by confining pressure. Normal stress and confining pressure were then raised to 20 and 15 MPa, respectively, and
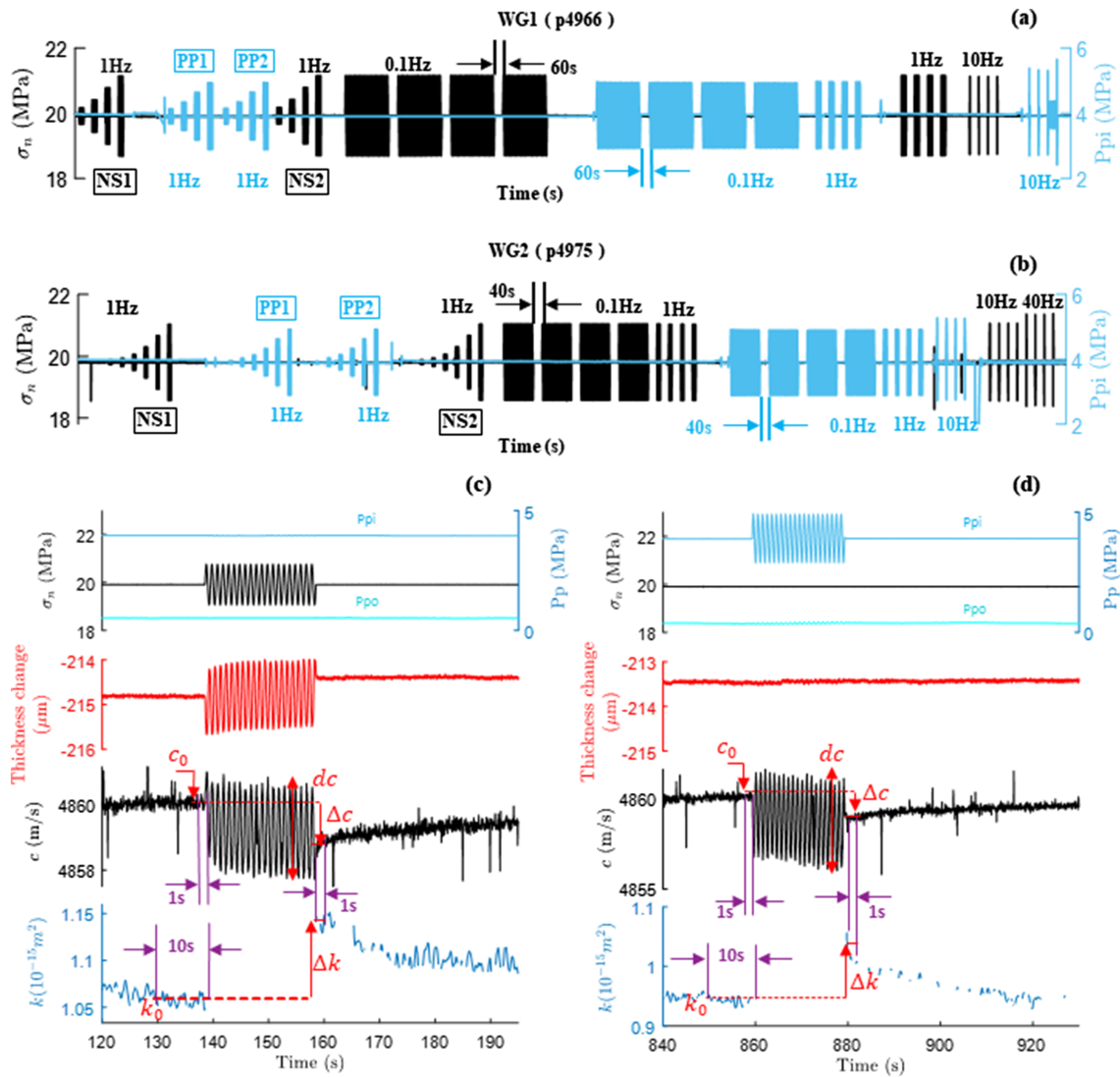
Figure 2. Overview of imposed normal stress σ_n and pore pressure P_p oscillations on the fractured sample for (a) WG1 (experiment p4966) and (b) WG2 (experiment p4975). Small horizontal arrows indicate hold times in unit of seconds. Examples of observed relative velocity and permeability change due to (c) normal stress (σ_n) oscillation and (d) pore pressure (P_p) oscillation. The velocity/permeability changes are calculated using the measured values before and after each oscillation averaged over the time windows shown in this figure. The missing data points in the permeability measurements are a result of discarding data corresponding to inlet/outlet flow rates different from each other by more than 5% (violating the assumption of steady flow and the use of Darcy's law).

maintained constant via servocontrol. The next step was to apply the inlet (P_{pi} = 4 MPa) and outlet (P_{po} = 2 MPa) pore pressures. Given the low permeability of the intact granite (<10^{-20} m^2) and the small applied pressure difference, no measurable flow was observed at this initial stage. Once all fluid pressures and solid stresses were applied, ultrasonic data acquisition was initiated using the Vantage^{TM} Research Ultrasound system (Verasonics®). The sample was then fractured in situ by increasing the shear stress at constant normal stress while making continuous measurements of fluid flow and ultrasonic properties. After locking the vertical piston (no displacement allowed), we executed the dynamic stressing protocol illustrated in Figure 2a.

All forces, displacements, and fluid pressures were measured continuously throughout the experiment with a 24-bit analog to digital converter at 10 kHz—and later averaged to recording rates of 100 or 1,000 Hz depending on the experimental protocol. Active ultrasonic data were recorded simultaneously at a rate of 25 MHz. The continually monitored mechanical, pore pressure, and ultrasonic data were time stamped

and fully synchronized. We determined the evolution of permeability and elastic properties in response to dynamic stressing using the techniques described below.

2.1. Dynamic (Effective) Stress Stimulation

The fractured samples were dynamically perturbed via pore pressure (P_p) and normal stress (σ_n) oscillations. Following the procedure described by Candela et al. (2015), pore pressure oscillations were achieved by oscillating P_{pi} while holding P_{po} constant. Conversely, normal stress oscillations were applied by oscillating the horizontal piston of the load frame at prescribed amplitude and frequency. As depicted in Figure 2a, multiple sets of P_p and σ_n oscillations of varying amplitude (up to about ±1 MPa) and frequency (0.1, 1, 10, and 40 Hz) were applied to investigate the repeatability as well as amplitude and frequency dependencies of the measured response. Similar parameters were used for P_p and σ_n oscillation sets in order to apply similar effective stress perturbations and allow making comparisons between P_p and σ_n stimulations.

2.2. Permeability Measurements

We measured flow rates independently at the inlet (Q_i) and outlet (Q_o) using the outputs of LVDTs on the pressure intensifiers. After verifying the steady state flow condition ($Q_i - Q_o \leq 5\%$), Darcy's law was used to calculate permeability k:

$$k = \frac{\mu L}{S} \frac{Q}{\Delta P_p}$$

where $Q = 1/2(Q_i+Q_o)$ is the average flow rate (m^3/s), μ is the fluid viscosity (10^{-3} Pa s) at 20 °C, L is the flow path given by the length of the sample (50 mm), and S is the cross section perpendicular to the flow path (45×26 mm^2). Here k is the bulk permeability of the sample including the permeability of fracture and its surrounding impermeable matrix (Faoro et al., 2009; Im et al., 2018). Alternatively, we could have calculated the permeability of the fracture itself (Ishibashi et al., 2018; Zhang et al., 2017). Both definitions would produce the same trends here, since we are not concerned with the absolute permeability of the fracture, but the relative change due to dynamic stressing.

2.3. Active Ultrasonic Measurements

Ultrasonic waves transmitted through the fracture were recorded continuously in each experiment. Half-cycle sinusoidal pulses with an amplitude of 40 V and frequency of 500 kHz were emitted consecutively from each transmitting transducer (nine piezoelectric disks arranged in a 3×3 matrix embedded within the right-hand loading block in Figure 1b) with a pulse repetition frequency of 100 or 1,000 Hz during the low and high frequency (≥ 10 Hz) stress oscillations, respectively. The waveforms were amplified (~40 dB) and recorded for all the receiving transducers (12 piezoelectric disks arranged in a 4×3 matrix embedded within the left-hand loading block in Figure 1b). We activated up to the full array of 9 transmitter and 12 receivers; however, in this paper, we focus on the results from a single transmitter-receiver pair obtained in two experiments. The ultrasonic waveforms are reduced to obtain the evolution of wave velocity before, during and after the imposed effective stress oscillations. As shown in Figure S1, we calculate the time shift by cross correlating each waveform with a reference waveform recorded at the unperturbed stress state. The peak of the cross-correlation function is fitted by a parabola to obtain subsampling frequency resolution. The reported wave velocity c is calculated from the time shift after accounting for changes in thickness (Figures 2c and 2d).

3. Results

The experimental data are analyzed to independently obtain the nonlinear elastodynamic response of the fractured rock as well as permeability changes due to imposed perturbations in effective stress. We used the ultrasonic records together with the strain measurements to calculate the former, whereas flow rate data were reduced to obtain the latter.

3.1. Nonlinear Elastodynamic Response

We use two parameters to quantify the nonlinearity of the fractured samples. The first is the relative velocity change ($\Delta c/c_0$) defined as the percent change in velocity due to the imposed oscillation. We calculate $\Delta c/c_0$ from the velocity before (c_0) and after (c) each oscillation averaged over 1-s time windows
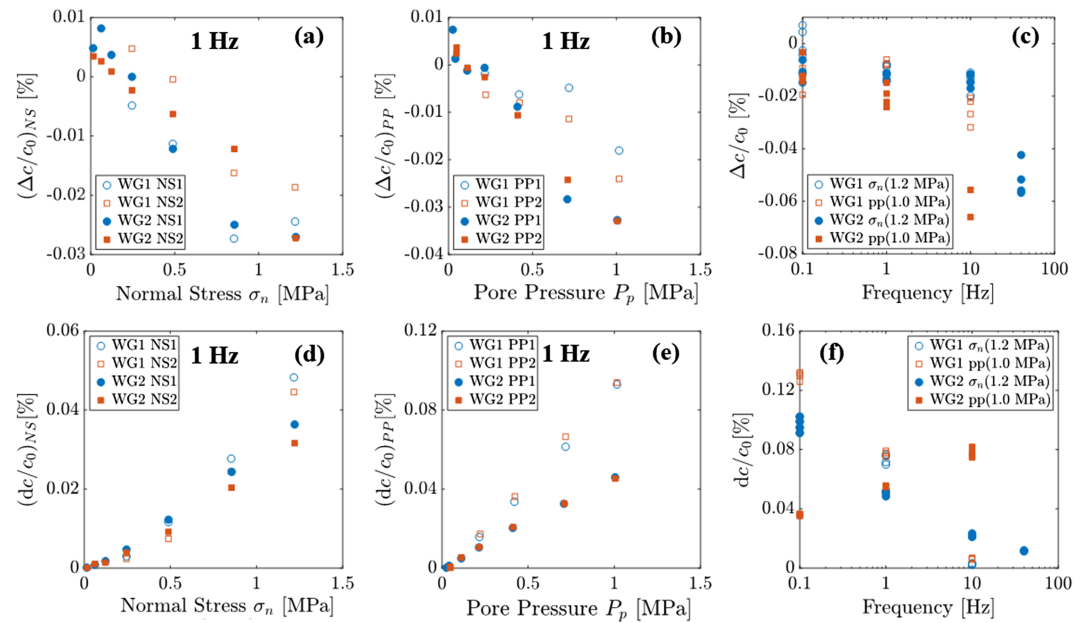
Figure 3. Dependencies of relative velocity change $\Delta c/c_0$ (a–c) and average velocity change amplitude dc/c_0 (d–f) on the amplitude and frequency of normal stress and pore water pressure oscillations. Each figure combines the results obtained in two different experiments on two Westerly granite samples, WG1 (p4966) and WG2 (p4975). The amplitude dependency is measured for two sets of 1-Hz normal stress oscillations (NS1 and NS2 shown in Figures 1a and 1b) as well as two sets of 1-Hz pore water pressure oscillations (PP1 and PP2 shown in Figures 1a and 1b). The frequency dependency is measured for the largest amplitudes, that is, 1.2-MPa normal stress and 1.0-MPa pore water pressure oscillations.

(Figures 2c and 2d). At a given oscillation amplitude, the more negative the $\Delta c/c_0$ (greater absolute value), the more nonlinear is the material. A second nonlinearity measure is the amplitude of velocity oscillations, averaged over the oscillation duration and normalized by preoscillation velocity c_0. Similar to $\Delta c/c_0$, a larger magnitude of dc/c_0 at a given oscillation amplitude is an indication of higher nonlinearity.

We quantify the nonlinear elastodynamic response of fractured rock using the dependence of $\Delta c/c_0$ and dc/c_0 on dynamic stress amplitude and frequency (Figure 3). Here we focus on two Westerly granite samples WG1 (experiment p4966) and WG2 (experiment p4975) and a single transmitter-receiver pair (Figure 3). The relative velocity change $\Delta c/c_0$ scales with the amplitude of both 1-Hz normal stress and 1-Hz pore pressure oscillations except at the highest amplitudes, where it plateaus (Figures 3a and 3b). This is because we use the same oscillation duration for all amplitudes, and therefore, at high amplitudes, the velocity oscillations may not reach a steady state. Thus, the measured $\Delta c/c_0$ may underestimate the true velocity offset for large oscillation amplitudes. The relative velocity changes $\Delta c/c_0$ for the two samples and for the first and second set of oscillations in each experiment are comparable, indicating reproducibility of the measurements. The larger difference between $\Delta c/c_0$ values for the two normal stress oscillation sets may be due to the oscillation sequence; the normal stress oscillations are separated by two consecutive pore pressure oscillations. Finally, the frequency dependence of $\Delta c/c_0$ for 1.2-MPa normal stress and 1-MPa pore pressure oscillation sets shown in Figure 3c suggests a general increase in nonlinearity with frequency; the increase is first subtle but becomes pronounced at higher frequencies. This trend is in accord with our previous observations in intact Berea sandstone (Rivière et al., 2016). The measured frequency dependencies for the two samples are more similar for normal stress than for pore pressure oscillations. This discrepancy could be due to the fact that the diffusion of pore pressure oscillations from inlet to outlet (only the inlet pressure is being oscillated) is slow relative to the period of oscillation for frequencies higher than 1 Hz—changing the loading distribution. Note that no data are available for WG1 at 40 Hz.

The parameter dc/c_0 scales linearly with the oscillation amplitude for both WG1 and WG2. Similar to $\Delta c/c_0$, dc/c_0 values fall in the same range for both samples and exhibit good repeatability especially for the two consecutive sets of pore pressure oscillations. However, the dependency of dc/c_0 on frequency is different from
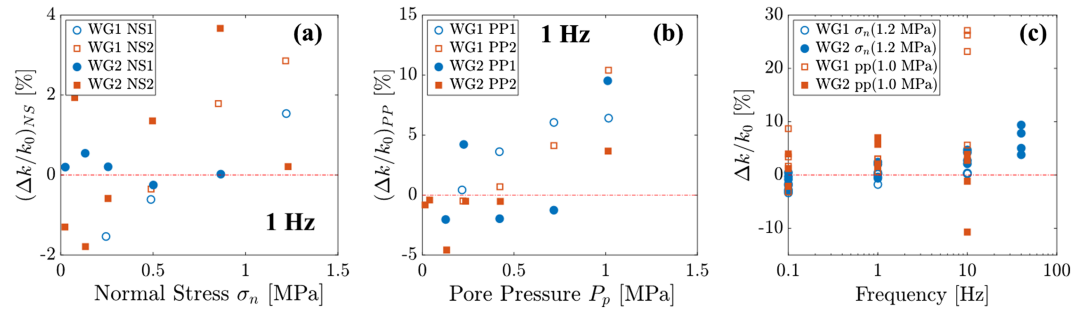
Figure 4. Dependency of relative permeability change $\Delta k/k_0$ on the amplitude (a and b) and frequency (c) of normal stress and pore water pressure oscillations in two different experiments on two Westerly granite samples, WG1 (p4966) and WG2 (p4975). The amplitude-dependency is measured for two sets of 1-Hz normal stress oscillations (NS1 and NS2 shown in Figures 1a and 1b) as well as two sets of 1-Hz pore water pressure oscillations (PP1 and PP2 shown in Figures 1a and 1b). The frequency dependency is measured for 1.2-MPa normal stress and 1.0-MPa pore water pressure oscillations.

that observed for $\Delta c/c_0$. For normal stress oscillations, dc/c_0 for both samples decreases as the frequency increases from 0.1 to 10 Hz. The observed trend for pore pressure oscillations is different for the two samples; dc/c_0 decreases with the frequency of pore pressure oscillations for WG1 but increases for WG2. It should be noted that the anomalous trend for WG2 is only observed for this particular transmitter-receiver pair; for the other pairs, dc/c_0 decreases with the pore pressure oscillation frequency as well.

3.2. Changes in Permeability Due to Normal Stress and Pore Pressure Oscillations

The relative change in permeability $\Delta k/k_0$ is defined as the perfect change in permeability due to the imposed normal stress or pore pressure oscillation, normalized by the preoscillation permeability (Candela et al., 2014). As shown in Figures 1c and 1d, the preoscillation permeability k_0 and the postoscillation permeability $k = k_0 + \Delta k$ are calculated by averaging the measured values over 10- and 1-s time windows, respectively. The discontinuities in permeability measurements shown in Figures 1c and 1d correspond to the data points for which inlet/outlet flow rate difference exceeds the 5% threshold.

The dependency of $\Delta k/k_0$ on the amplitude and frequency of normal stress and pore pressure oscillations are shown in Figure 4. The red dashed lines in these figures at $\Delta k/k_0 = 0$ mark the boundary between permeability increase and decrease due to the imposed oscillation. Despite the scatter in the data (Figures 4a and 4b), the relative permeability change $\Delta k/k_0$ generally scales with the amplitude of 1-Hz normal stress and pore pressure oscillations. Small-amplitude oscillations may even result in a decrease in permeability, whereas large-amplitude oscillations generally increase the permeability. Comparing Figures 4a and 4b, the pore pressure oscillations appear to be more effective in permeability enhancement ($\Delta k/k_0 > 0$) than the normal stress oscillations by a factor of ~2.5, particularly for WG1. The frequency dependence of permeability changes for normal stress and pore pressure oscillations are presented in Figure 4c. Note that the permeability changes are larger for the 10-Hz fluid pressure oscillations as well as the 40-Hz normal stress oscillations. The permeability change increases, albeit slightly, with frequency. The only exception is the decrease in $\Delta k/k_0$ for WG2, when we increase the fluid pressure oscillations from 1 to 10 Hz (blue squares).

4. Discussion

Many rock types exhibit strongly nonlinear mesoscopic elastic (NME) behavior, such that the stiffness is highly strain dependent for strains greater than ~10^{-6} (Guyer & Johnson, 2009). The presence of fractures increases the local compliance and thus enhances elastic nonlinearity. The nonlinearity of a fractured interface is dictated by the surface roughness and fracture stress (e.g., Jin et al., 2018). One of the elastodynamic signatures of NME materials is the strain dependency of elastic wave velocity (see Figures 2c and 2d). The strain-induced changes in wave velocity ($\Delta c/c_0$ and dc/c_0) would be null for a perfectly linear elastic material because the elastic moduli in a linear elastic medium are constant and thus, the wave velocity is strain invariant. However, in an NME material, the wave velocity drops instantaneously upon dynamic stressing. Our data support these statements. Our measurements of the relative changes in wave velocity $\Delta c/c_0$ show an initial sudden drop, which is known to be related to the hysteretic nonlinearity parameter
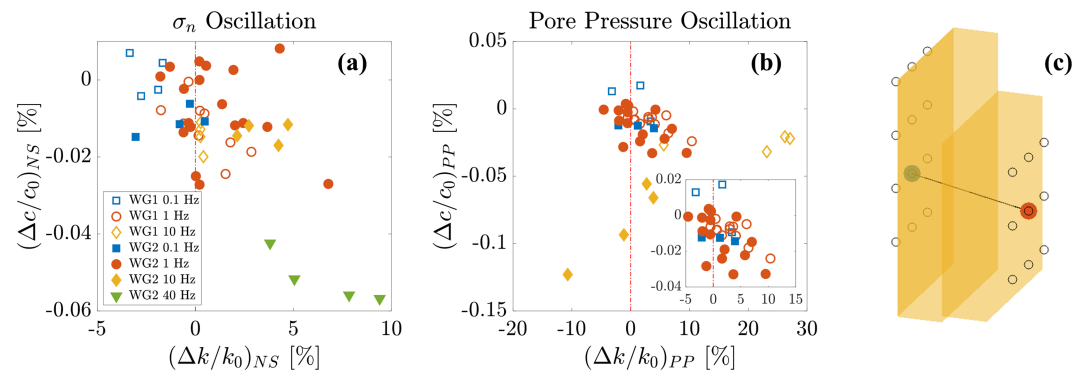
Figure 5. Correspondence between nonlinearity and permeability change due to (a) normal stress and (b) pore water pressure oscillations. The inset in (b) excludes the data corresponding to 10-Hz oscillations. The nonlinearity is expressed in terms of $\Delta c/c_0$, relative change in velocity due to imposed effective stress oscillations. (c) The position of the two ultrasonic transducers used in the study relative to the fracture plane. The wavelength for a 500-kHz pulse in Westerly Granite (~5,000 m/s) is about 1 cm. The area probed (~1 cm^2) therefore corresponds to roughly 8% of the total fracture plane.

α (Guyer & Johnson, 2009). This drop is followed by oscillatory fluctuations of wave velocity, which reach a nonequilibrium steady state for sufficiently long perturbations (Rivière et al., 2015). The wave velocity oscillations occur primarily at the perturbation frequency (f) but may also include higher order harmonics, nf for $n = 2,3,...$,etc. The amplitude of velocity oscillations dc/c_0 (Figures 2c and 2d) is related to the nonlinear parameter β that is typically estimated via the second harmonic (e.g., Rivière et al., 2013, 2015). Once the perturbation ceases, the wave velocity slowly relaxes to the preoscillation value c_0—a phenomenon known as slow dynamics (Shokouhi et al., 2017; TenCate et al., 2000).

We document the correspondence between transient changes in elastic wave properties and permeability during dynamic stressing (Figure 5). Changes in wave speed are calculated for a single pair of transducers (Figure 5c). With the exception of a few points corresponding to pore pressure oscillations at 10 Hz, relative velocity and permeability change appear to be well correlated. In other words, the increased nonlinearity (more negative $\Delta c/c_0$) is associated with larger permeability enhancement (more positive $\Delta k/k_0$) and vice versa. The observed correlation is remarkable considering that we measure wave velocity between only one pair of transducers, thus sampling a small area of the fractured interface, whereas permeability depends on the entire fracture length (Figure 1c). Interestingly, the correlation exists for both normal stress and pore pressure oscillations, although pore pressure oscillations are generally more effective in enhancing permeability. As noted previously (Figure 4), small-amplitude oscillations of both normal stress and pore pressure may result in a decrease in permeability.

The results presented in Figure 5 support the initial hypothesis of a link between the nonlinear elastodynamic behavior and hydraulic properties of fractured rock. One explanation for this linkage is the strong dependence of both properties on fracture aperture and roughness; specifically, on the changes in asperity contact areas that correlate with transient closure of the fracture as a result of the imposed stress oscillations. The measured nonlinearity parameter, the transient drop in wave velocity $\Delta c/c_0$, is a result of instantaneous loss of contact between asperities over the rough fracture interface. Once the oscillation is removed, the contacts begin to heal, resulting in a slow logarithmic-in-time recovery of wave velocity toward preperturbation values. Permeability changes could also result from changes in fracture aperture during the oscillations (Candela et al., 2015; Im et al., 2018). To further examine this hypothesis, it is useful to investigate whether $\Delta c/c_0$ or $\Delta k/k_0$ correlate with measured sample thickness changes due to imposed oscillations. As shown in Figure S4, while a subset of $(\Delta c/c_0)_{\rm NS}$ and thickness data seem to be correlated, the overall correlation is rather weak. The correlation between $(\Delta k/k_0)_{\rm NS}$ and thickness change is even weaker. In addition, no correlation is observed for either $(\Delta c/c_0)_{\rm PP}$ or $(\Delta k/k_0)_{\rm PP}$. These observations suggest that changes in fracture aperture are not the sole driving mechanism, especially for pore pressure oscillations.

Previous work shows that unclogging of fracture flow conduits is the primary mechanism of transient changes in permeability during fluid pressure oscillations (Candela et al., 2014, 2015). For example, the

unclogging of temporary blockages in the fluid path is used to explain the modulation of transient permeability changes with pore pressure oscillation amplitude. Also, the first oscillations in a multioscillation set are the most effective, with subsequent oscillations yielding smaller changes in permeability. Yet this mechanism does not adequately explain observations of reduced permeability due to normal stress oscillations (Candela et al., 2015). Unclogging of the fracture aperture may indeed be one of the underlying mechanisms behind our observations as well. However, unlike in Candela et al. (2015), we observe an increase in permeability for both pore pressure and normal stress oscillations of large enough amplitude. It can be argued that sufficiently strong oscillations are capable of clearing the fracture aperture from fines. On the one hand, this will increase the fluid flow, which in turn translates into permeability enhancement ($\Delta k/k_0 > 0$). On the other hand, unclogging may reduce the contact area at the fracture interface, which may decrease the transmitted wave velocity ($\Delta c/c_0 < 0$), depending on whether the clogging agents are simply covering pore throats or in intimate contact with one or both fracture surfaces. Nevertheless, this mechanism does not explain the permeability loss ($\Delta k/k_0 < 0$) after imposing low-amplitude oscillations, especially when it is coupled with a decrease in wave velocity ($\Delta c/c_0 < 0$). Also, unlike in Candela et al. (2015), we find that the first oscillation is not always the most effective, an observation that does not support the unclogging hypothesis (Figure S5). A study of permeability change versus flow rate amplitude *during* effective stress oscillations does not yield a clear correlation (see Figure S6). This is contrary to the results by Candela et al., 2014, who found a strong dependence of permeability change on flow rate during fluid pressure oscillations with Berea Sandstone. It is notable that in our study, the correlation is stronger for pore pressure oscillations and that the fluid flow amplitudes during normal stress oscillations are 2 orders of magnitude smaller than those during fluid pressure oscillations. Considering all the above observations, one may conclude that unclogging is not the only potential mechanism but merely one of many potential active mechanisms that explain permeability evolution due to pore pressure oscillations. To investigate the extent to which unclogging is responsible for the observed phenomena, additional work is needed to examine the downstream water chemistry and the presence of fines during dynamic stressing.

5. Conclusions

We present observations on the coupling between elastic stiffness and permeability transients due to dynamic stressing. Understanding this relationship can help illuminate key processes governing flow in fractured reservoirs, energy production, and subsurface waste disposal. Our experiments reveal a correlation between changes in permeability and wave velocity due to dynamic stressing via both normal stress and pore pressure oscillations. Within the range of our experimental parameters, oscillations of larger-amplitude and higher frequency tend to be more effective in increasing permeability. Also, pore pressure oscillations are more effective in permeability enhancement than normal stress oscillations of the same amplitude and frequency. Our observations suggest that dynamic stressing is more likely to enhance the permeability of fractured rocks that exhibit greater elastic nonlinearity.

Aperture change and unclogging are candidate mechanisms to explain our observations. The former is likely to be dominant during normal stress oscillations while the latter appears to dominate during pore pressure oscillations. Future experiments on prefractured and saw-cut samples of known roughness will quantify the role of aperture change for changes in dynamic stiffness and permeability. We will also look for fines in the downstream effluent before and after dynamic stressing in order to better understand the role of unclogging in promoting permeability enhancement.

References

Batzle, M. L., Han, D.-H., & Hofmann, R. (2006). Fluid mobility and frequency-dependent seismic velocity—Direct measurements. *Geophysics*, *71*(1), N1–N9. https://doi.org/10.1190/1.2159053

Berkowitz, B. (2002). Characterizing flow and transport in fractured geological media: A review. *Advances in Water Resources*, *25*(8), 861–884. https://doi.org/10.1016/S0309-1708(02)00042-8

Berryman, J. G., Berge, P. A., & Bonner, B. P. (2002). Estimating rock porosity and fluid saturation using only seismic velocities. *Geophysics*, *67*(2), 391–404. https://doi.org/10.1190/1.1468599

Brenguier, F., Campillo, M., Hadziioannou, C., Shapiro, N. M., Nadeau, R. M., & Larose, E. (2008). Postseismic relaxation along the San Andreas Fault at Parkfield from continuous seismological observations. *Science*, *321*(5895), 1478–1481. https://doi.org/10.1126/science.1160943

Brenguier, F., Campillo, M., Takeda, T., Aoki, Y., Shapiro, N. M., Briand, X., et al. (2014). Mapping pressurized volcanic fluids from induced crustal seismic velocity drops. *Science*, *345*(6192), 80–82. https://doi.org/10.1126/science.1254073

Brodsky, E. E., & Lajoie, L. J. (2013). Anthropogenic seismicity rates and operational parameters at the Salton Sea geothermal field. *Science*, *341*(6145), 543–546. https://doi.org/10.1126/science.1239213

Brown, S. R. (1987). Fluid flow through rock joints: The effect of surface roughness. *Journal of Geophysical Research*, *92*(B2), 1337–1347. https://doi.org/10.1029/JB092iB02p01337

Candela, T., Brodsky, E. E., Marone, C., & Elsworth, D. (2014). Laboratory evidence for particle mobilization as a mechanism for permeability enhancement via dynamic stressing. *Earth and Planetary Science Letters*, *392*, 279–291. https://doi.org/10.1016/j.epsl.2014.02.025

Candela, T., Brodsky, E. E., Marone, C., & Elsworth, D. (2015). Flow rate dictates permeability enhancement during fluid pressure oscillations in laboratory experiments: Dynamic permeability enhancement. *Journal of Geophysical Research: Solid Earth*, *120*, 2037–2055. https://doi.org/10.1002/2014JB011511

Carey, J. W., Lei, Z., Rougier, E., Mori, H., & Viswanathan, H. (2015). Fracture-permeability behavior of shale. *Journal of Unconventional Oil and Gas Resources*, *11*, 27–43. https://doi.org/10.1016/j.juogr.2015.04.003

Davis, S. D., & Pennington, W. D. (1989). Induced seismic deformation in the Cogdell oil field of west Texas. *Bulletin of the Seismological Society of America*, *79*(5), 1477–1495.

Deichmann, N., & Giardini, D. (2009). Earthquakes induced by the stimulation of an enhanced geothermal system below Basel (Switzerland). *Seismological Research Letters*, *80*(5), 784–798. https://doi.org/10.1785/gssrl.80.5.784

Durham, W., & Bonner, B. (1995). *Closure and fluid flow in discrete fractures. In Fractured and jointed rock masses* (Vol. 441, p. 446). Brookfield, Netherlands: Balkema Rotterdam.

Elkhoury, J. E., Brodsky, E. E., & Agnew, D. C. (2006). Seismic waves increase permeability. *Nature*, *441*(7097), 1135–1138. https://doi.org/10.1038/nature04798

Elkhoury, J. E., Niemeijer, A., Brodsky, E. E., & Marone, C. (2011). Laboratory observations of permeability enhancement by fluid pressure oscillation of in situ fractured rock. *Journal of Geophysical Research*, *116*, B02311. https://doi.org/10.1029/2010JB007759

Ellsworth, W. L. (2013). Injection-induced earthquakes. *Science*, *341*(6142). https://doi.org/10.1126/science.1225942

Faoro, I., Elsworth, D., & Marone, C. (2012). Permeability evolution during dynamic stressing of dual permeability media. *Journal of Geophysical Research*, *117*, B01310. https://doi.org/10.1029/2011JB008635

Faoro, I., Niemeijer, A., Marone, C., & Elsworth, D. (2009). Influence of shear and deviatoric stress on the evolution of permeability in fractured rock. *Journal of Geophysical Research*, *114*, B01201. https://doi.org/10.1029/2007JB005372

Frash, L. P., Carey, J. W., Lei, Z., Rougier, E., Ickes, T., & Viswanathan, H. S. (2016). High-stress triaxial direct-shear fracturing of Utica shale and in situ X-ray microtomography with permeability measurement. *Journal of Geophysical Research: Solid Earth*, *121*, 5493–5508. https://doi.org/10.1002/2016JB012850

Frohlich, C. (2012). Two-year survey comparing earthquake activity and injection-well locations in the Barnett Shale, Texas. *Proceedings of the National Academy of Sciences*, *109*(35), 13934–13938. https://doi.org/10.1073/pnas.1207728109

Gale, J. E. (1982). *The effects of fracture type (induced versus natural) on the stress-fracture closure-fracture permeability relationships*. In ARMA-82-290, (p. 9). Berkeley, California: ARMA: American Rock Mechanics Association.

Guéguen, Y., & Schubnel, A. (2003). Elastic wave velocities and permeability of cracked rocks. *Tectonophysics*, *370*(1–4), 163–176. https://doi.org/10.1016/S0040-1951(03)00184-7

Guyer, R. A., & Johnson, P. A. (2009). *Nonlinear mesoscopic elasticity: The complex behaviour of rocks, soil, concrete*. Hoboken, NJ: John Wiley & Sons.

Healy, J. H., Rubey, W. W., Griggs, D. T., & Raleigh, C. B. (1968). The Denver earthquakes. *Science*, *161*(3848), 1301–1310.

Hofmann, R., Xu, X., Batzle, M., Prasad, M., Furre, A.-K., & Pillitteri, A. (2005). Effective pressure or what is the effect of pressure? *The Leading Edge*, *24*(12), 1256–1260. https://doi.org/10.1190/1.2149644

Holland, A. A. (2013). Preliminary analysis of the 2013 Love County earthquake swarm. *Oklahoma Geological Survey Open-File Report OF1*, *2013*, 30.

Horton, S. (2012). Disposal of hydrofracking waste fluid by injection into subsurface aquifers triggers earthquake swarm in Central Arkansas with potential for damaging earthquake. *Seismological Research Letters*, *83*(2), 250–260. https://doi.org/10.1785/gssrl.83.2.250

Im, K., Elsworth, D., & Fang, Y. (2018). The influence of preslip sealing on the permeability evolution of fractures and faults. *Geophysical Research Letters*, *45*, 166–175. https://doi.org/10.1002/2017GL076216

Ishibashi, T., Elsworth, D., Fang, Y., Riviere, J., Madara, B., Asanuma, H., et al. (2018). Friction-stability-permeability evolution of a fracture in granite. *Water Resources Research*, *54*, 9901–9918. https://doi.org/10.1029/2018WR022598

Jin, J., Rivière, J., Ohara, Y., & Shokouhi, P. (2018). Dynamic acousto-elastic response of single fatigue cracks with different microstructural features: An experimental investigation. *Journal of Applied Physics*, *124*(7), 075303. https://doi.org/10.1063/1.5036531

Li, Y.-G., Chen, P., Cochran, E. S., Vidale, J. E., & Burdette, T. (2006). Seismic evidence for rock damage and healing on the San Andreas Fault associated with the 2004 M 6.0 Parkfield earthquake. *Bulletin of the Seismological Society of America*, *96*(4B), S349–S363. https://doi.org/10.1785/0120050803

Li, Y.-G., Vidale, J. E., Aki, K., Xu, F., & Burdette, T. (1998). Evidence of shallow fault zone strengthening after the 1992 M7.5 Landers, California, earthquake. *Science*, *279*(5348), 217–219. https://doi.org/10.1126/science.279.5348.217

Mavko, G. (2013). Relaxation shift in rocks containing viscoelastic pore fluids. *Geophysics*, *78*(3), M19–M28. https://doi.org/10.1190/geo2012-0272.1

McGarr, A., Bekins, B., Burkardt, N., Dewey, J., Earle, P., Ellsworth, W., et al. (2015). Coping with earthquakes induced by fluid injection. *Science*, *347*(6224), 830–831. https://doi.org/10.1126/science.aaa0494

McNamara, D. E., Hayes, G. P., Benz, H. M., Williams, R. A., McMahon, N. D., Aster, R. C., et al. (2015). Reactivated faulting near Cushing, Oklahoma: Increased potential for a triggered earthquake in an area of United States strategic infrastructure. *Geophysical Research Letters*, *42*, 8328–8332. https://doi.org/10.1002/2015GL064669

Nara, Y., Meredith, P. G., Yoneda, T., & Kaneko, K. (2011). Influence of macro-fractures and micro-fractures on permeability and elastic wave velocities in basalt at elevated pressure. *Tectonophysics*, *503*(1), 52–59. https://doi.org/10.1016/j.tecto.2010.09.027

Niu, F., Silver, P. G., Daley, T. M., Cheng, X., & Majer, E. L. (2008). Preseismic velocity changes observed from active source monitoring at the Parkfield SAFOD drill site. *Nature*, *454*(7201), 204–208. https://doi.org/10.1038/nature07111

Petrovitch, C. L., Nolte, D. D., & Pyrak-Nolte, L. J. (2013). Scaling of fluid flow versus fracture stiffness. *Geophysical Research Letters*, *40*, 2076–2080. https://doi.org/10.1002/grl.50479

Pyrak-Nolte, L. J., Myer, L. R., Cook, N. G. W., & Witherspoon, P. A. (1987). Hydraulic and mechanical properties of natural fractures in low-permeability rock (No. LBL-22718; CONF-870815-2). Lawrence Berkeley Lab., CA (USA). Retrieved from https://www.osti.gov/biblio/6406367

Pyrak-Nolte, L. J., & Nolte, D. D. (2016). Approaching a universal scaling relationship between fracture stiffness and fluid flow. *Nature Communications*, *7*, 10663. https://doi.org/10.1038/ncomms10663

Raleigh, C. B., Healy, J. H., & Bredehoeft, J. D. (1976). An experiment in earthquake control at Rangely, Colorado. *Science*, *191*(4233), 1230–1237. https://doi.org/10.1126/science.191.4233.1230

Rivière, J., Pimienta, L., Scuderi, M., Candela, T., Shokouhi, P., Fortin, J., et al. (2016). Frequency, pressure, and strain dependence of nonlinear elasticity in Berea Sandstone. *Geophysical Research Letters*, *43*, 3226–3236. https://doi.org/10.1002/2016GL068061

Rivière, J., Renaud, G., Guyer, R. A., & Johnson, P. A. (2013). Pump and probe waves in dynamic acousto-elasticity: Comprehensive description and comparison with nonlinear elastic theories. *Journal of Applied Physics*, *114*(5), 054905. https://doi.org/10.1063/1.4816395

Rivière, J., Shokouhi, P., Guyer, R. A., & Johnson, P. A. (2015). A set of measures for the systematic classification of the nonlinear elastic behavior of disparate rocks. *Journal of Geophysical Research: Solid Earth*, *120*, 1587–1604. https://doi.org/10.1002/2014JB011718

Shi, Z., Zhang, S., Yan, R., & Wang, G. (2018). Fault zone permeability decrease following large earthquakes in a hydrothermal system. *Geophysical Research Letters*, *45*(3), 1387–1394.

Shi, Y., Liao, X., Zhang, D., & Liu, C. P. (2019). Seismic waves could decrease the permeability of the shallow crust. Geophysical Research Letters.

Shokouhi, P., Rivière, J., Guyer, R. A., & Johnson, P. A. (2017). Slow dynamics of consolidated granular systems: Multi-scale relaxation. *Applied Physics Letters*, *111*(25), 251604. https://doi.org/10.1063/1.5010043

Simpson, D. W., Leith, W. S., & Scholz, C. H. (1988). Two types of reservoir-induced seismicity. *Bulletin of the Seismological Society of America*, *78*(6), 2025–2040.

Sminchak, J., & Gupta, N. (2003). Aspects of induced seismic activity and deep-well sequestration of carbon dioxide. *Environmental Geosciences*, *10*(2), 81–89. https://doi.org/10.1306/eg.04040302009

TenCate, J. A., Smith, E., & Guyer, R. A. (2000). Universal slow dynamics in granular solids. *Physical Review Letters*, *85*(5), 1020–1023. https://doi.org/10.1103/PhysRevLett.85.1020

van der Elst, N. J., Savage, H. M., Keranen, K. M., & Abers, G. A. (2013). Enhanced remote earthquake triggering at fluid-injection sites in the midwestern United States. *Science*, *341*(6142), 164–167. https://doi.org/10.1126/science.1238948

Walsh, F. R., & Zoback, M. D. (2015). Oklahoma's recent earthquakes and saltwater disposal. *Science Advances*, *1*(5), e1500195. https://doi.org/10.1126/sciadv.1500195

Weingarten, M., Ge, S., Godt, J. W., Bekins, B. A., & Rubinstein, J. L. (2015). High-rate injection is associated with the increase in US mid-continent seismicity. *Science*, *348*(6241), 1336–1340. https://doi.org/10.1126/science.aab1345

Witherspoon, P. A., Wang, J. S. Y., Iwai, K., & Gale, J. E. (1980). Validity of Cubic Law for fluid flow in a deformable rock fracture. *Water Resources Research*, *16*(6), 1016–1024. https://doi.org/10.1029/WR016i006p01016

Wu, C., Peng, Z., & Ben-Zion, Y. (2009). Non-linearity and temporal changes of fault zone site response associated with strong ground motion. *Geophysical Journal International*, *176*(1), 265–278. https://doi.org/10.1111/j.1365-246X.2008.04005.x

Xu, X., Hofmann, R., Batzle, M., & Tshering, T. (2006). Influence of pore pressure on velocity in low-porosity sandstone: Implications for time-lapse feasibility and pore-pressure study: Influence of pore pressure on velocity in sandstone. *Geophysical Prospecting*, *54*(5), 565–573. https://doi.org/10.1111/j.1365-2478.2006.00569.x

Ye, Z., & Ghassemi, A. (2018). Injection-induced shear slip and permeability enhancement in granite fractures. *Journal of Geophysical Research: Solid Earth*, *123*(10), 9009–9032.

Zhang, F., Fang, Y., Elsworth, D., Wang, C., & Yang, X. (2017). Evolution of friction and permeability in a propped fracture under shear. *Geofluids*, *2017* [Research article]. https://doi.org/10.1155/2017/2063747

Zhang, H., Wan, Z., Feng, Z., & Wu, J. (2018). Shear-induced Permeability Evolution of Sandstone Fractures. Geofluids, 2018.

Zimmerman, R. W., & Bodvarsson, G. S. (1996). Hydraulic conductivity of rock fractures. *Transport in Porous Media*, *23*(1), 1–30. https://doi.org/10.1007/BF00145263

Zoback, M. D. (2012). Managing the seismic risk posed by wastewater disposal. *Earth*, *57*(4), 38.

Zoback, M. D., & Gorelick, S. M. (2012). Earthquake triggering and large-scale geologic storage of carbon dioxide. *Proceedings of the National Academy of Sciences*, *109*(26), 10164–10168. https://doi.org/10.1073/pnas.1202473109